Moisture-Insensitive, Phase-Stable Indium-Based Metal Halides and Their Light-Emitting Applications

Zhe Tang, Xuan Meng, Hongyuan Zhao, Sujun Ji, Qiujie Wang, Tianxin Bai, Ruiling Zhang, Junke Jiang, Claudine Katan, Jacky Even, et al.

Moisture-Insensitive, Phase-Stable Indium-Based Metal Halides and Their Light-Emitting Applications

Zhe Tang,[1,a] Xuan Meng,[1,a] Hongyuan Zhao,[1] Sujun Ji,[1] Qiujie Wang,[1] Tianxin Bai,[1] Ruiling Zhang,[1] Junke Jiang,[2] Claudine Katan,[3] Jacky Even*,[2] and Feng Liu*,[1]

[1]Institute of Molecular Sciences and Engineering, Institute of Frontier and Interdisciplinary Science, Shandong University, Qingdao 266237, P. R. China

[2]Univ Rennes, INSA Rennes, CNRS, Institut FOTON - UMR 6082, F-35000 Rennes, France

[3]Univ Rennes, ENSCR, CNRS, ISCR-UMR 6226, F-35000 Rennes, France

[a]These authors contributed equally to this work

*E-mail: fenglau189@sdu.edu.cn;jacky.even@insa-rennes.fr

Abstract

Ternary indium (In)-based metal halides are gaining increased attention as promising lead (Pb)-free alternatives for light-emitting applications owing to their broadband emission, high photoluminescence quantum yields (PLQYs), and a high oxidation stability of In^{3+}. However, most of the pure In-based compositions suffer from instability against moisture and thermal stress, leading to a rapid material degradation and hence their optical properties. Herein, we present a new kind of organic-inorganic hybrid In-based metal halide, BA_6InCl_9 ($BA^+ = C_4H_{11}N^+$), which exhibits stable crystal structure and material composition at both ambient (over 2 months) and heating conditions (up to 200 °C). Besides, the Huang-Rhys factor of ~4.94 determined for BA_6InCl_9 is considerably smaller than most Pb-free perovskites with broadband emission, which suggests an exceptionally weak exciton-phonon coupling in these crystals. By trace amounts of Sb^{3+} doping, PLQY of the BA_6InCl_9 single crystals can be greatly improved from ~25% to 95%, paving the way for the fabrication of high-efficiency optoelectronic devices based on BA_6InCl_9. UV-pumped LEDs fabricated with Sb-doped BA_6InCl_9 powder crystals exhibit bright orange-red emission with an external quantum efficiency of 0.12%, which retains about 50% of the initial luminance

after 380 min of continuous operation in ambient air. We foresee that our study will prompt future research on In-based metal halides and their use in stable light-emitting applications.

Keywords: stable indium-based metal halide; lead-free perovskite derivative; coordinating water-free indium halide; organic-inorganic metal halide; down-conversion LEDs

Introduction

Lead (Pb)-free low-dimensional metal halide perovskites have drawn tremendous interest for many emerging applications owing to their fascinating optoelectronic properties including broadband emission, long radiative lifetime, and tunable band structure.[1-3] Different from those of three-dimensional (3D) metal halides, the low-dimensional compositions generally possess large lattice distorsions associated with strong electron-phonon coupling, which have been suggested to be favorable for the formation of radiative self-trapped excitons (STEs) and to contribute to the broadband emission.[4] In addition, due to strong quantum confinement and large exciton binding energies, the low-dimensional metal halides usually exhibit higher radiative recombination efficiency, making them promising candidates for the next-generation of light-emitting diodes (LEDs), photodetectors, and lasers.[3, 5]

Recently, a variety of Pb-free low-dimensional metal halides including Bi-, Sb-, In-, Cu-, and Ag-based compositions were produced by low-cost solution methods, several of which have shown excellent fluorescent properties with high photoluminescence quantum yields (PLQYs) approaching 100%.[5-8] Despite their high PL efficiency, there is still great potential to be exploited in enhancing application prospects of these Pb-free luminescent materials. Emissive layers with high stability both in ambient atmosphere and at elevated temperatures could be desired for functional devices which may run under a harsh environment such as oxygen, moisture, and heating.[9] For example, cuprous (Cu^{+})-based metal halides especially Cl-based ones like $Cs_3Cu_2Cl_5$ show appealing photophysical properties, but similar to Sn^{2+}-based halide perovskites, this kind of material can be easily oxidized, leading to fast structural collapse at ambient

conditions.[10-11] Another example, Sb-based metal halide, $Cs_3Sb_2Cl_9$, exhibits structural instabilities, leading to pure trigonal crystal phase at ≤ 85 °C and orthorhombic phase at ≥ 130 °C.[12] As for In-based halide compounds, a formidable challenge facing the use of these materials is their dynamic water-stimuli-responsive properties, *i.e.*, they readily transform into hydrated phases by uptake of coordinating water in air, meanwhile, easily lose it under mild heat treatment. For instance, the recently reported 0D Cs_3InCl_6 easily absorbs water and undergoes a phase change from orthorhombic Cs_3InCl_6 to monoclinic $Cs_2InCl_5 \cdot H_2O$.[13] Although these coordinating water-containing products including the Br-based compositions, such as $Cs_2InBr_5 \cdot H_2O$, $(C_8NH_{12})_6InBr_9 \cdot H_2O$, and $(C_7H_8N_3)_3InBr_6 \cdot H_2O$, still emit light, it should be noted that they are thermally unstable. Due to the presence of coordinating water molecules, these compounds begin to transform at around 110 °C and irreversibly decompose at around 150 °C depending on the A-site molecules contained in the structure.[14-17] Although such moisture/heat sensitivity renders these materials useful for water detection, a wider utilization in optoelectronics where a high ambient stability is of paramount importance, for example, LEDs, photodetectors, and lasers, *etc.*, may be largely hindered.

In this work, we report a new kind of coordinating water-free, ternary In-based metal halide, BA_6InCl_9 ($BA^+ = C_4H_{11}N^+$), which exhibits high resistance to thermal stress up to 200 °C and maintains stable crystal structure under ambient atmosphere (relative humidity, *RH* ~40%) for over 2 months. Moreover, unlike most other In-based ternary halides, BA_6InCl_9 exhibits strong electron-phonon coupling processes, which is beneficial to both radiative recombination and broadband emission. Optical properties of the BA_6InCl_9 single crystals can be facilely modified by Sb^{3+} doping, which boosts PLQY of these orange-red-emissive materials from ~25% to 95%. Experimental results and density functional theory (DFT) calculations reveal that an appropriate amount of Sb^{3+} doping does not change the crystal structure of BA_6InCl_9, but it induces a below band gap optical transition related an electronic state in the band gap of the host structure. It leads to an enhanced light harvesting and hence an improved STE emission. UV-pumped LEDs fabricated with BA_6InCl_9:Sb powder crystals exhibit broadband emission from 500 to 900 nm with an external quantum efficiency (EQE) of 0.12%,

which retains ~50% of the initial luminance after 380 min of operation in ambient air. Our findings unambiguously show that the newly developed BA_6InCl_9:Sb compound is a promising single-component luminescent material for orange-red LED applications.

Results and Discussion

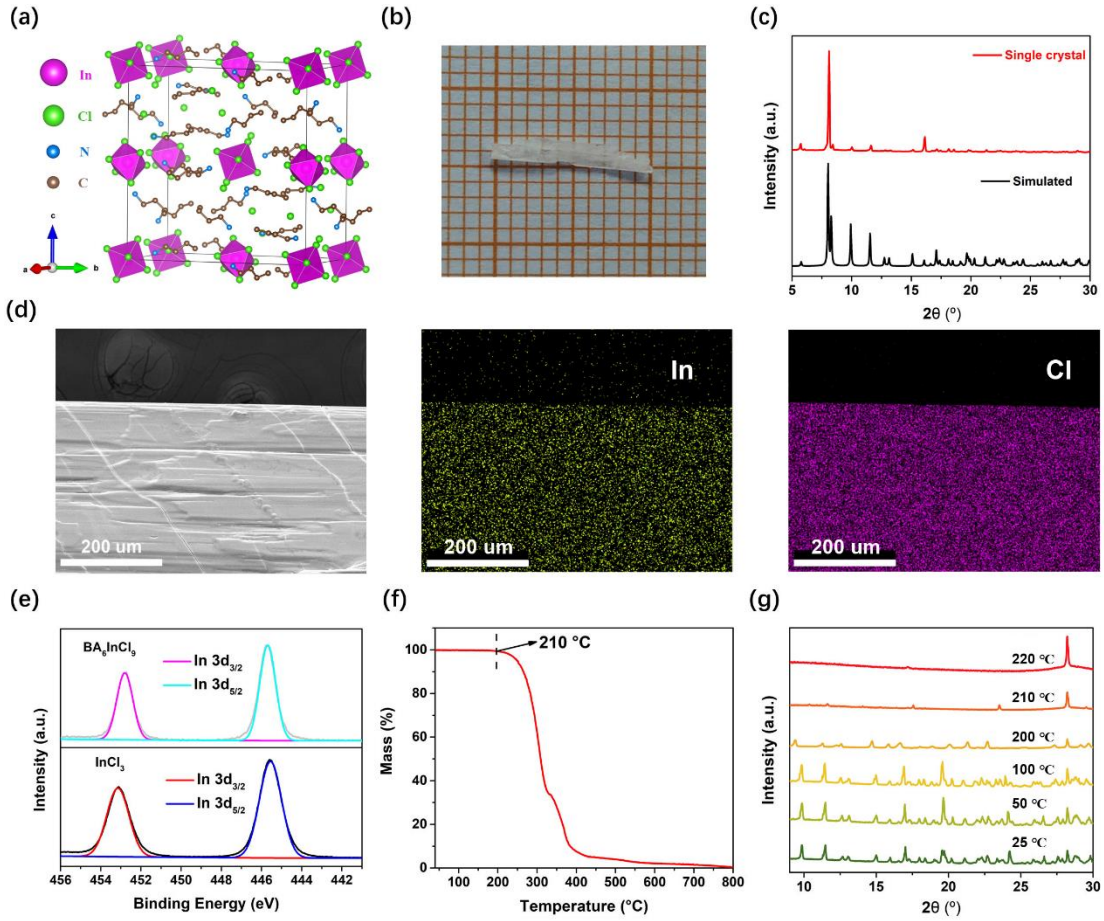

Figure 1. (a) Crystal structure of BA_6InCl_9, created with VESTA software based on crystallographic information obtained by X-ray single crystal structural analyses. A CIF file is provided in the SI. (b) Photograph of a typical single crystal taken under ambient light. (c) Powder XRD pattern of the ground single crystal and the simulated one for powder BA_6InCl_9. (d) Element distribution analysis of BA_6InCl_9 single crystals by EDS mapping. (e) In 3d XPS spectrum of the BA_6InCl_9 single crystals. Data of the as-bought $InCl_3$ powder was used for comparison. (f) TG curve and (g) variable-temperature XRD patterns of the BA_6InCl_9 single crystals.

In a typical synthesis of BA_6InCl_9 single crystals, powder mixture containing BACl and

$InCl_3$ was first dissolved in a concentrated hydrochloric acid. The solution was then placed on a hot plate and heated at 150 °C for 30 min. After cooling down to room temperature, the precipitated crystals were taken out, washed by N,N-dimethylformamide and dried with a vacuum oven at 60 °C (more experimental details can be found in Supporting Information, SI). Single-crystal X-ray diffraction (XRD) analyses performed on the as-grown crystals reveal a specific chemical composition of BA_6InCl_9, which crystallizes in the monoclinic *I*2/c space group and features a 0D structure. In this material, each $[InCl_6]^{3-}$ octahedron is spatially separated by the wide-band-gap organic framework of BA^+ (see Figure 1a; Tables S1-6 of the SI). BA_6InCl_9 forms single crystals that present 1-cm-long and 0.2-cm-wide rods (Figure 1b). XRD pattern of the finely ground powders from single crystals shows the same features as the simulated one, suggesting the high purity and uniformity of the synthesized crystals (Figure 1c). Elemental mapping image acquired by energy dispersive X-ray spectroscopy (EDS) displays that the In and Cl elements are uniformly distributed in the crystals (Figure 1d). Further, X-ray photoelectron spectroscopy (XPS) measurement was carried out to confirm the presence of In element in its expected oxidation state. The measured high-resolution In 3d spectrum consists of a pair separated by the In 3d spin-orbit splitting (Figure 1e), each of which has well-resolved single component at 450.9 and 442.5 eV, respectively, in good agreement with the In 3d spectrum of the as-bought $InCl_3$ powder. To evaluate thermal stability of the prepared sample, thermogravimetric (TG) analysis was performed. It is seen from Figure 1f that the thermal degradation is multi-stage. The first stage begins at about 200 °C and the crystal loses 70% of its initial mass, corresponding to the loss of BACl; the second stage which shows a mass loss of ~30% can be then assigned to the evaporation of $InCl_3$. The above TG results agree well with the mass ratio of $BACl/InCl_3$ in BA_6InCl_9, confirming the high thermal stability of the prepared single crystals. To investigate the possible phase transformation during heat treatment in TG measurement, we have further acquired their variable-temperature XRD patterns, shown in Figure 1g. It is seen that the main diffraction peaks of the BA_6InCl_9 single crystals undergo a slight shift towards lower angles with continuous heating to 200 °C, which can be caused by a certain degree of

thermal expansion of the lattice parameters upon heating. However, importantly, no other secondary phases can be observed at elevated temperatures, confirming that these coordinating water-free metal halides do have a high resistance to thermal stress. Note that such thermal stability is comparable to that of the widely studied $MAPbCl_3$ perovskite, which maintains stable crystal structure at around 200 °C.[18]

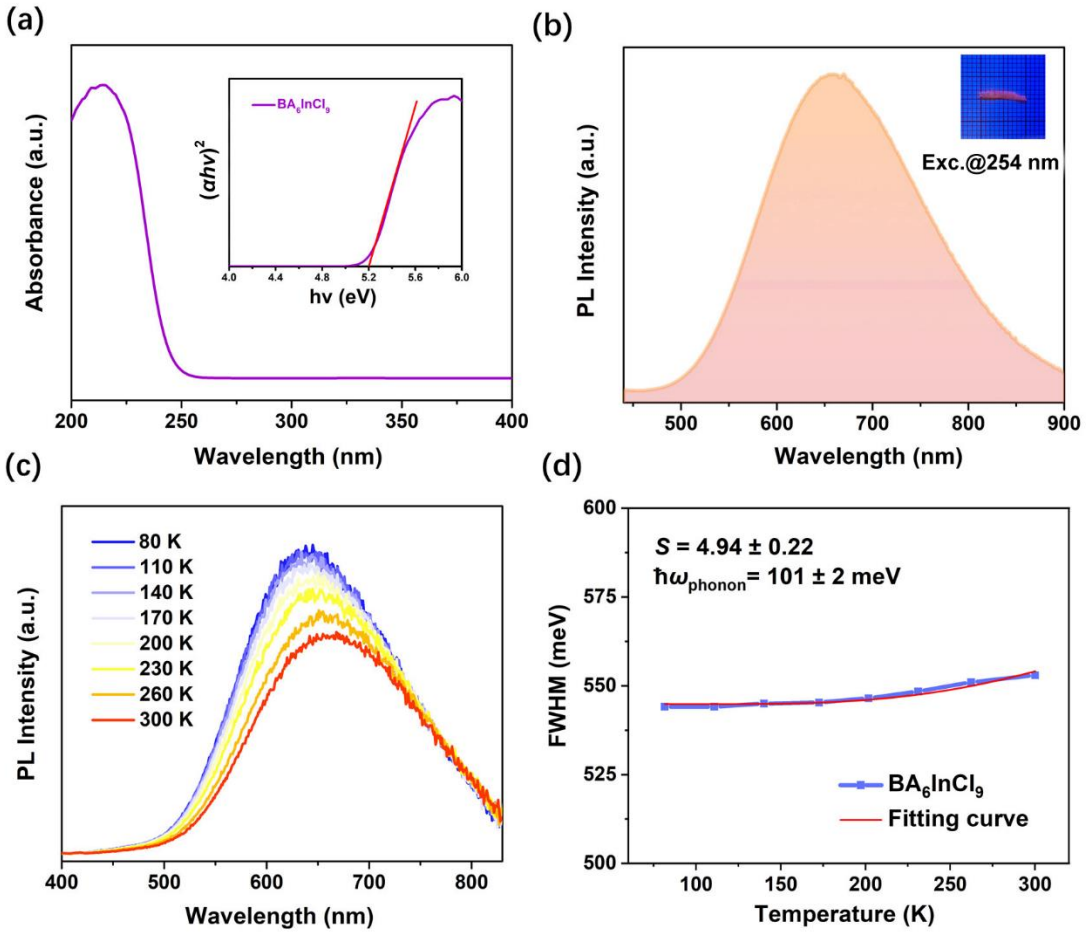

Figure 2. (a) UV-vis absorption spectrum of the BA_6InCl_9 single crystals. Inset shows the Tauc's plot for the sample. (b) PL spectrum of the BA_6InCl_9 single crystals excited at 270 nm. Inset shows photograph of a typical sample taken under 254-nm UV light. (c) Temperature-dependent PL spectra from 80 to 300 K and (d) FWHM as a function of temperature.

Optical properties of the as-synthesized crystals were then investigated by UV-vis absorption and PL spectra. Figure 2a shows that the UV-vis absorption spectrum of the BA_6InCl_9 single crystals features a very strong and steep absorption onset, which is

indicative of the direct band-edge absorption of the material. Inset shows the Tauc's plot for the sample, from which a band gap of 5.2 eV was extracted assuming direct band gap optical transitions. The PL excitation (PLE) spectrum shown in Figure S1 indicates that the BA_6InCl_9 single crystal can be excited below the optical band gap derived from absorption, with 240~360 nm radiation and has two optimal excitation wavelengths around 270 and 330 nm. It is worth mentioning that the recorded PLE spectrum for BA_6InCl_9 does not seem to comply with the measured absorption spectrum, which shows cut-off edge at about 250 nm. One possible reason for this is that the as-prepared BA_6InCl_9 single crystals do contain electronic states that can be excited by 240~360 nm radiation, yet their concentration is too low to generate significant difference during UV-vis absorption measurement.

Figure 2b records PL spectrum of the BA_6InCl_9 bulk crystals excited at 270 nm (one of the optimal excitation wavelengths), which exhibits broadband emission from 500~900 nm along with a large Stokes shift of ~350 nm. To probe into the underlying mechanism of the broadband emission of BA_6InCl_9 single crystals, emission wavelength-dependent PLE spectra and excitation wavelength-dependent PL spectra were examined. It was found that both PLE and PL spectra exhibit identical shapes at various emission (from 550 to 850 nm) and excitation wavelengths (from 260 to 350 nm) (Figure S2-3), which is indicative of the fact that the broadband emission originates from the same excited states and rules out the possibility of In^{3+} ionoluminescence with different excited-state levels.

Actually, the broadband emission accompanied by a large Stokes shift observed in our samples has been widely reported in other low-dimensional In-based metal halides and it is generally believed to be derived from STEs.[14, 16, 19] STEs are those photo-excited electron-hole pairs whose coupling with lattice is strong enough to cause local elastic distortion in the lattice surrounding them. As a result, transient, light-induced trap states form below the conduction band, affording a broad emission with a large Stokes shift. The well-known Huang-Rhys factor (S) is an important parameter to evaluate the strength of electron-phonon coupling. Generally, according to the magnitude of the S, the electron-phonon coupling coefficients can be divided into

extremely weak coupling (S < 1), medium coupling (S = 1~5), and strong coupling (S > 5) cases. Note that an overly large S will increase the possibility of nonradiative recombination, which is unfavorable for the efficient STE emission.[4] To study the electron-phonon coupling in our BA_6InCl_9 single crystals, Huang-Rhys factor was extracted by using the following equation:

$$FWHM = 2.36\sqrt{S}\hbar\omega_{photon}\sqrt{\coth\frac{\hbar\omega_{photon}}{2k_BT}} \quad (1)$$

where FWHM is the PL full width at half maximum, $\hbar\omega_{phonon}$ is the phonon frequency, and k_B is the Boltzmann constant. Figure 2c reports the temperature-dependent PL spectra for BA_6InCl_9, where we see a noticeable decrease in PL intensity from 80 to 300 K. It is noteworthy that such negative correlation between PL emission and temperature is quite common in these luminescent materials, which can be due to the thermal quenching caused by the increased thermally populated vibrational states at high temperatures.[20] The FWHM data, derived from the temperature-dependent PL spectra, was plotted in Figure 2d. FWHM changes monotonously with the increasing temperature. It broadens significantly from 80 to 300 K, indicative of an increased optical phonon scattering with temperature. By fitting FWHM curve using equation 1, the *S* factor and $\hbar\omega_{phonon}$ are extracted to be 4.94 ± 0.22 and 101 ± 2 meV, respectively. Notably, the derived *S* factor is one of the lowest values reported for these emissive materials with broadband emission, including Ag^+-, In^{3+}-, Cd^{2+}-, and Cu^+-based ternary metal halides, which usually have *S* value ranging from 8 to 40.[21-26] Meanwhile, it is still larger than those band-edge emissive materials, such as $CsPbBr_3$ (3.2), CdSe (1.0), and ZnSe (0.3). Such *S* value reflects an adequate standard of exciton-phonon coupling interaction in BA_6InCl_9, which is conducive to producing broadband emission while maintaining a high PLQY.[4]

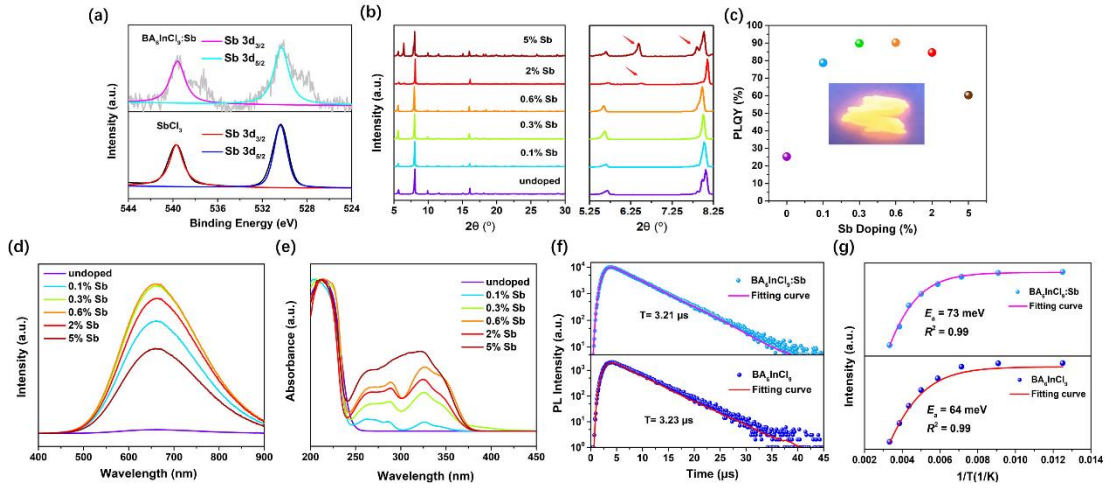

Figure 3. (a) Sb 3d XPS spectrum of the Sb-doped BA_6InCl_9 single crystals. Data of the as-bought $SbCl_3$ powder was used for comparison. (b) Powder XRD patterns, (c) dependence of PLQY, and (d) PL spectra of BA_6InCl_9 single crystals with different Sb^{3+} doping levels. Inset in figure 3c shows typical photograph of 0.5 mol% Sb-doped samples taken under 254-nm UV light, which show brighter emission compared to the pristine ones. (e) UV-vis absorption spectra of 0~5 mol% Sb^{3+}-doped BA_6InCl_9. (f) TRPL curve and (g) PL peak intensity as a function of temperature recorded for the pristine and 0.5 mol% Sb-doped BA_6InCl_9 single crystals.

Luminescence efficiency of the BA_6InCl_9 single crystals was evaluated by measuring their PLQYs using a commercial Hamamatsu setup. PLQY of the as-prepared BA_6InCl_9 single crystals was measured to be ~25%. We note that such luminous efficiency has already exceeded most other In-based compounds, including the widely investigated 3D $Cs_2AgInCl_6$ and $Cs_2NaInCl_6$, which typically have low PLQYs < 10%.[27-28] Yet it is still significantly lower than Pb-based perovskites, whose PLQYs have reached as high as ~100%.[29-30] The mechanism behind the relatively low luminous efficiency observed in these In-based metal halides has been intensively studied and attributed mainly to the presence of a parity-forbidden transition originating from the unoccupied In 5s orbitals, which largely limits their achievable PLQYs.[16-17] To better utilize the intrinsic light-emitting property of BA_6InCl_9 and to enhance their future prospects and potential in LED applications, we seek to further boost their PL performance by Sb^{3+} doping, a common strategy which is typically employed to enhance their PLQYs.[15-16, 31] Detailed

synthesis of Sb-doped crystals can be found in SI. The successful incorporation of the Sb^{3+} ions in BA_6InCl_9 was confirmed by XPS, where we see a clear Sb^{3+} signal in the doped sample (Figure 3a). XRD measurements suggest that the original crystal structure of BA_6InCl_9 is well retained with Sb doping levels between 0 and ~0.6 mol%, as the main diffraction peaks are unchanged and no extra diffractions can be observed (Figure 3b) (the actual content of Sb in crystals is determined by inductively coupled plasma-mass spectrometry, ICP-MS). However, the diffraction peaks shift toward lower 2θ angle as the doping level increases, which points to the fact that the Sb dopant has induced a lattice expansion for the host material. Such lattice expansion of the BA_6InCl_9 crystals is actually unexpected given the fact that Sb^{3+} (0.90 Å) is smaller than In^{3+} (0.94 Å), replacement of which would tend to contract the lattice.[16-17] One possible reason is that the Sb^{3+} dopant does not form the same crystal structure as that of BA_6InCl_9, instead the dopant may have formed BA-Sb-Cl networks with larger lattice parameters. As the Sb doping level reaches 2~5 mol%, there are extra peaks appearing at 6.3° and 7.8° (marked by the red arrow), and meanwhile the overall diffraction peaks shift back to higher 2θ angles, indicating a certain degree of phase change in BA_6InCl_9 single crystals.

In addition to crystal structure, the Sb^{3+} doping strategy has also caused a dramatic change in PL properties of the obtained crystals. In particular, by appropriate content of Sb doping (0.3~0.6 mol%), PLQY of the BA_6InCl_9 single crystals was improved from 25% to 95% without affecting their spectral range and symmetry (Figure 3c-d), making them one of the most efficient orange-red-emitters reported to date. To better understand the effect of Sb doping on optical properties of the BA_6InCl_9 single crystals, UV-vis absorption spectra of the undoped and 0~5 mol% Sb^{3+}-doped crystals were first recorded and compared. It is seen from Figure 3e that compared to the pristine sample, the Sb^{3+}-doped crystals show an obvious absorption signal in the range 250-375 nm, implying that Sb^{3+} doping has led to a stronger optical absorption for the BA_6InCl_9 single crystals. Moreover, the absorption spectra calculated from DFT also show an obvious absorption peak at ~370 nm with Sb^{3+} doping (Figure S4), which qualitatively agrees with the experimental results. However, the Sb-doped samples retain almost the

same PLE profile to that of the undoped ones, except that the optimal excitation wavelength has moved from 270 to 330 nm (Figure S5). A similar change in optical properties was reported in other In-based metal halides that contain trace amounts of Sb^{3+}, which is believed to result from the extra excitation associated with the $^1S_0 \rightarrow {}^3P_1$ transitions of $[SbCl_6]^{3-}$ in the forbidden energy gap of the host structure.[15-16, 31] Such enhanced absorption generates more carriers that could be trapped, producing more STEs and thus contributing to higher luminous efficiency.[15-16]

To shed more light on how carriers in Sb-doped crystals recombine through radiative process, time-resolved PL (TRPL) measurements were conducted. Figure 3f shows the typical TRPL curve for the pristine and optimally Sb-doped single crystals monitoring the same emission peak at 660 nm. It is found that PL decay curve of the doped crystals is nearly identical to that of the pristine one, both can be well-fitted by a mono-exponential decay function with lifetime constant of 3.23 μs. Such long-lived PL lifetime is typical characteristic of the STE emission and the same radiative lifetime indicates that the Sb dopants do not influence trap states in BA_6InCl_9 single crystals. Importantly, this PL decay result also serves to support the deduction that the low PLQYs of the pristine BA_6InCl_9 single crystals is not caused by their trap states and the Sb doping strategy does not improve their PLQYs through a defect-passivation way.

By fitting and comparing the temperature-dependent integrated PL intensity, we have also examined the influence of Sb doping on exciton thermal activation energy of the BA_6InCl_9 single crystals, which is closely related to materials' radiative recombination process. Figure 3g presents the integrated PL intensity for both samples as a function of inverse temperature, which can be fitted by using the following Arrhenius equation:[32]

$$I(T) = \frac{I_0}{1 + A\exp(\frac{-E_a}{k_B T})} \quad (2)$$

where $I(T)$ is the integrated PL intensity at T (K), A is a constant, and E_a is the thermal activation energy. It is found that the pristine BA_6InCl_9 possesses E_a of 64 meV, while that of the Sb-doped sample has E_a value of 73 meV. The enhanced thermal activation energy would also contribute to a higher PLQY because it helps excitons to be localized

at ambient temperature for efficient bound and STE emission.[4, 33]

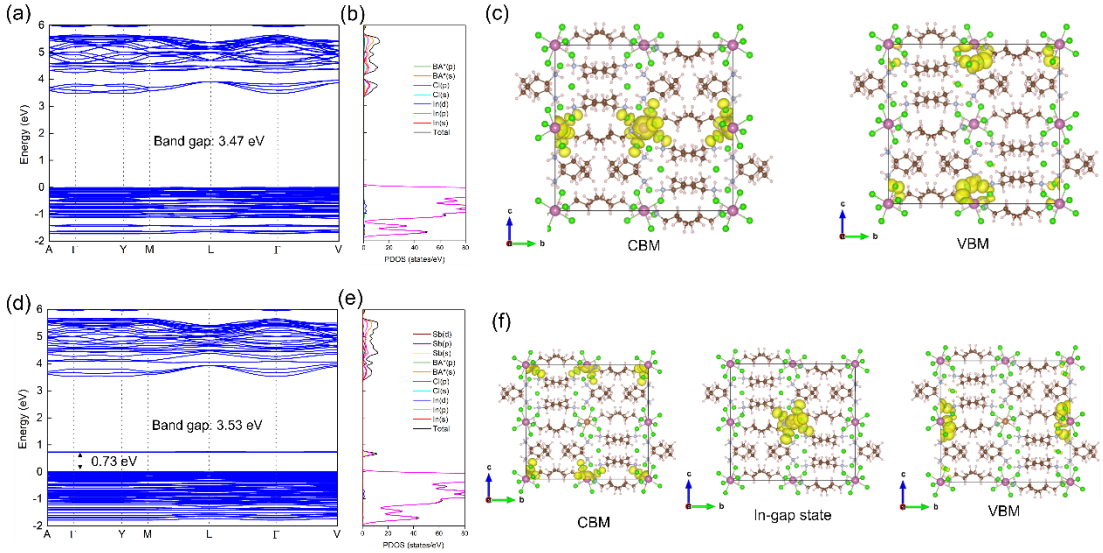

Figure 4. The calculated (a) band structure, (b) PDOS and (c) partial charge density for the CBM and VBM of BA_6InCl_9. The calculated (d) band structure, (e) PDOS and (f) partial charge density for the CBM, in-gap state, and VBM of Sb-doped BA_6InCl_9.

To get an insight into the electronic properties of the Sb-doped BA_6InCl_9 single crystals, DFT calculations were performed. The calculated electronic band structure of BA_6InCl_9 shows flat dispersions consistent with the low-dimensionality and high band gap of the material (Figure 4a). Note that the calculated band gap (3.47 eV) is underestimated, which is expected as the regular DFT calculations usually underestimate band gaps of the semiconductors.[34-35] The conduction band minimum of BA_6InCl_9 features a moderated curvature, and the valence band maximum (VBM) reveals an almost flat band, both indicating very weak inter motif coupling as expected for these structurally 0D metal halides. This can be understood as a consequence of spatial isolation of $[InCl_6]^{3-}$ octahedra by BA^+ molecules. The projected density of states (PDOS) (Figure 4b) shows that the CBM of BA_6InCl_9 is composed mainly of In-s and Cl-p orbitals, whereas their VBM mainly relates to Cl-p orbitals, as indicated by the partial charge density (Figure 4c). Figure 4d-e show that the incorporated Sb generates an in-gap electronic state above VBM, while the CBM only undergoes moderated changes. This also suggests that the Sb dopant modifies the optical

absorption of the host as shown in Figure S4.

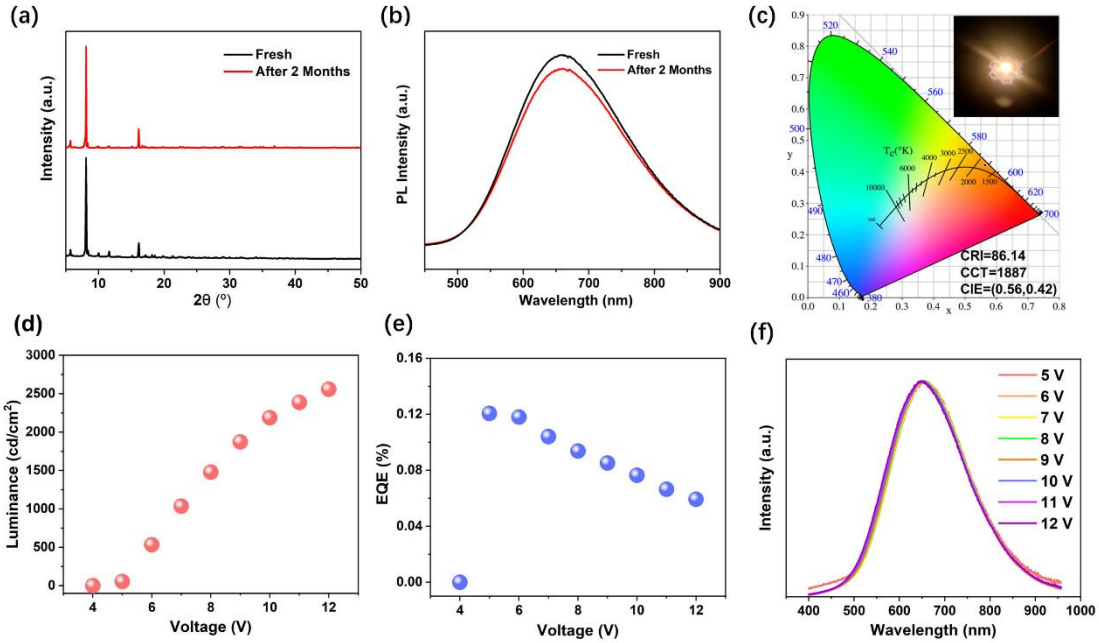

Figure 5. (a) XRD patterns and (b) PL spectra of the doped BA_6InCl_9 after 2 months of storage in the open air (~40% *RH*, 25 °C). (c) CIE coordinates and the main luminous parameters of the UV-pumped BA_6InCl_9:Sb LEDs. Inset shows photograph of a typical device in operation. (d) Luminous intensity, (e) EQE, and (f) PL spectra of the fabricated LEDs working under different bias voltages in the open air (~40% *RH*, 25 °C).

Stabilities of a luminescent material especially under ambient conditions are of paramount importance for assessing their potential for light-emitting applications. Phase stability of the Sb^{3+}-doped crystals was evaluated by XRD measurement. As shown in Figure 5a, XRD patterns of the doped BA_6InCl_9 crystals remain unchanged even after 2-month storage in the open air (*RH* ~40%). Such high stability is further confirmed by measuring their PL spectrum, which remains intact and maintains high PLQY of 90% (Figure 5b).

The high PLQYs and stable crystal structure make these luminescent materials to be promising candidates for efficient LEDs. We therefore prepared UV-pumped LEDs by directly pressing the BA_6InCl_9:Sb crystal powders onto a commercial ultraviolet LED chip (310 nm), without using epoxy or silica encapsulation for protection. Figure 5c

shows the photograph of the as-fabricated LEDs that emit bright and uniform light, which features Commission Internationale de l´Eclairage (CIE) color coordinates of (0.56, 0.42) and correlated color temperature of 1887 K. The device shows a brightness up to 2600 cd/m^2 at a driving voltage of 12 V and highest EQE of 0.12% at ~5 V (Figure 5d-e). Importantly, the emission color demonstrates high stability. Figure 5f shows the normalized PL spectra of the fabricated LEDs, which remain almost constant when the voltage level is varied from 5 to 12 V. To study the operational stability of the as-prepared UV-pumped LEDs, we further tracked the luminance of the unencapsulated devices at a driving voltage of ~6 V (Figure S6). It is shown that LEDs retain about 50% of the initial luminance after 380 min of continuous operation in ambient air, inferior than that of the commercial LED chips (Figure S7). Since luminous efficiency of the BA_6InCl_9:Sb emitters has negative correlation with temperature (shown in Figure 3g), the decreased luminance of the UV-pumped LEDs is not unexpected because the used commercial LED chips will be heated up after a continuous long-term work.

Conclusions

This work presents a new kind of Pb-free 0D hybrid metal halide, $(BA)_6InCl_9$. Unlike most other In-based metal halides which suffer from lack of resistance to moisture damage, the $(BA)_6InCl_9$ crystal is less reactive and susceptible to water attack, maintaining stable crystal structure under ambient conditions for over 2 months. Moreover, since $(BA)_6InCl_9$ single crystals do not contain coordinating water in the structure, stability against thermal stress is also considerably improved. Highly emissive $(BA)_6InCl_9$ single crystals with PLQY approaching 95% were achieved by Sb^{3+} doping, an effective strategy that induces an extra excitation in the forbidden energy gap of the host structure. Down-conversion LEDs fabricated with Sb-doped $(BA)_6InCl_9$ powder crystals show high EQE of 0.12% and a good operational stability in ambient air. This work offers a promising alternative to Pb-based halide perovskites including promising optical performance and enhanced stability.

Associated Content

Supporting Information

Experimental details, computational details, cif file, PL spectra, and UV-pumped LED characteristics.

Author Information

Corresponding Author

*E-mail: fenglau189@sdu.edu.cn

Notes

The authors declare no competing financial interest.

Acknowledgements

This work was financially supported by National Natural Science Foundation of China (No. 22179072), the Natural Science Foundation of Shandong Province (No. ZR2021QF006), the Outstanding Youth Science Foundation of Shandong Province (Overseas) (No. 2022HWYQ-006), and the Qilu Youth Scholar Foundation of Shandong University (No. 62460082163114). Acknowledgements*** The work at Institut FOTON was performed within the frame of the M-ERA.NET project PHANTASTIC (R.8003.22), supported by the French national research agency (ANR) and received funding from Région Bretagne. J.E. acknowledges the financial support from the Institut Universitaire de France.

References

[1] H. Peng and B. Zou, Effects of Electron–Phonon Coupling and Spin–Spin Coupling on the Photoluminescence of Low-Dimensional Metal Halides. *J. Phys. Chem. Lett.,* 2022, **13**, 1752-1764.

[2] W. Chen, F. Zhang, C. Wang, M. Jia, X. Zhao, Z. Liu, Y. Ge, Y. Zhang and H. Zhang, Nonlinear Photonics Using Low-Dimensional Metal-Halide Perovskites: Recent Advances and Future Challenges. *Adv. Mater.,* 2021, **33**, 2004446.

[3] H.-P. Wang, S. Li, X. Liu, Z. Shi, X. Fang and J.-H. He, Low-Dimensional Metal Halide Perovskite Photodetectors. *Adv. Mater.,* 2021, **33**, 2003309.

[4] S. Li, J. Luo, J. Liu and J. Tang, Self-Trapped Excitons in All-Inorganic Halide Perovskites: Fundamentals, Status, and Potential Applications. *J. Phys. Chem. Lett.,* 2019, **10**, 1999-2007.

[5] Y. Han, S. Yue and B.-B. Cui, Low-Dimensional Metal Halide Perovskite Crystal Materials: Structure Strategies and Luminescence Applications. *Adv. Sci.,* 2021, **8**, 2004805.

[6] Y. Guo, B. Chen, X. Ren and F. Wang, Recent Advances in All-Inorganic Zero-Dimensional Metal Halides. *ChemPlusChem,* 2021, **86**, 1577-1585.

[7] P. Zhu and J. Zhu, Low-Dimensional Metal Halide Perovskites and Related Optoelectronic Applications. *Infomat,* 2020, **2**, 341-378.

[8] Z. Chu, X. Chu, Y. Zhao, Q. Ye, J. Jiang, X. Zhang and J. You, Emerging Low-Dimensional Crystal Structure of Metal Halide Perovskite Optoelectronic Materials and Devices. *Small Struct.,* 2021, **2**, 2000133.

[9] W. K. Bae, S. Brovelli and V. I. Klimov, Spectroscopic Insights into the Performance of Quantum Dot Light-Emitting Diodes. *MRS Bull.,* 2013, **38**, 721-730.

[10] W. Bai, S. Shi, T. Lin, T. Zhou, T. Xuan and R.-J. Xie, Near-Unity Cyan-Green Emitting Lead-Free All-Inorganic Cesium Copper Chloride Phosphors for Full-Spectrum White Light-Emitting Diodes. *Adv. Photonics Res.,* 2021, **2**, 2000158.

[11] S. Zhao, C. Chen, W. Cai, R. Li, H. Li, S. Jiang, M. Liu and Z. Zang, Efficiently Luminescent and Stable Lead-free Cs3Cu2Cl5@Silica Nanocrystals for White Light-Emitting Diodes and Communication. *Adv. Optical Mater.,* 2021, **9**, 2100307.

[12] A. Pradhan, S. C. Sahoo, A. K. Sahu and S. L. Samal, Effect of Bi Substitution on Cs3Sb2Cl9: Structural Phase Transition and Band Gap Engineering. *Crystal Growth & Design,* 2020, **20**, 3386-3395.

[13] P. Han, C. Luo, S. Yang, Y. Yang, W. Deng and K. Han, All-Inorganic Lead-Free 0D Perovskites by a Doping Strategy to Achieve a PLQY Boost from <2 % to 90 %. *Angew. Chem. Int. Ed.,* 2020, **59**, 12709-12713.

[14] L. Zhou, J.-F. Liao, Z.-G. Huang, J.-H. Wei, X.-D. Wang, W.-G. Li, H.-Y. Chen, D.-B. Kuang and C.-Y. Su, A Highly Red-Emissive Lead-Free Indium-Based Perovskite Single Crystal for Sensitive Water Detection. *Angew. Chem. Int. Ed.,* 2019, **58**, 5277-5281.

[15] X. Liu, X. Xu, B. Li, Y. Liang, Q. Li, H. Jiang and D. Xu, Antimony-Doping Induced Highly Efficient Warm-White Emission in Indium-Based Zero-Dimensional

Perovskites. *CCS Chem.,* 2020, **2**, 216-224.

[16] J. Lin, K. Liu, H. Ruan, N. Sun, X. Chen, J. Zhao, Z. Guo, Q. Liu and W. Yuan, Zero-Dimensional Lead-Free Halide with Indirect Optical Gap and Enhanced Photoluminescence by Sb Doping. *J. Phys. Chem. Lett.,* 2022, **13**, 198-207.

[17] Z. Li, G. Song, Y. Li, L. Wang, T. Zhou, Z. Lin and R.-J. Xie, Realizing Tunable White Light Emission in Lead-Free Indium(III) Bromine Hybrid Single Crystals through Antimony(III) Cation Doping. *J. Phys. Chem. Lett.,* 2020, **11**, 10164-10172.

[18] Z. Yuan, W. Huang, S. Ma, G. Ouyang, W. Hu and W. Zhang, A High Performance Perovskite CH3NH3PbCl3 Single Crystal Photodetector: Benefiting from an Evolutionary Preparation Process. *J. Mater. Chem. C,* 2019, **7**, 5442-5450.

[19] P. Han, W. Zhou, D. Zheng, X. Zhang, C. Li, Q. Kong, S. Yang, R. Lu and K. Han, Lead-Free All-Inorganic Indium Chloride Perovskite Variant Nanocrystals for Efficient Luminescence. *Adv. Optical Mater.,* 2022, **10**, 2101344.

[20] L. Lian, P. Zhang, G. Liang, S. Wang, X. Wang, Y. Wang, X. Zhang, J. Gao, D. Zhang, L. Gao, H. Song, R. Chen, X. Lan, W. Liang, G. Niu, J. Tang and J. Zhang, Efficient Dual-Band White-Light Emission with High Color Rendering from Zero-Dimensional Organic Copper Iodide. *ACS Appl. Mater. Inter.,* 2021, **13**, 22749-22756.

[21] Z. Ma, S. Lin, X. Ji, X. Chen, D. Wu and Z. Shi, Thermal-Evaporation-Deposited CsCu2I3 Films with Self-Trapped Excitons for Electrically Driven Yellow Light-Emitting Diodes. *J. Alloys Compd.,* 2023, **930**, 167462.

[22] X. Meng, S. Ji, Q. Wang, X. Wang, T. Bai, R. Zhang, B. Yang, Y. Li, Z. Shao, J. Jiang, K.-l. Han and F. Liu, Organic–Inorganic Hybrid Cuprous-Based Metal Halides for Warm White Light-Emitting Diodes. *Adv. Sci.,* 2022, 2203596.

[23] T. Tian, X. Xiong, Y. Zhao, H. Li, W. Wang and L. Wang, Ultra-Wideband Warm White Light Emission from Self-Trapped Excitons in CsAgCl2. *J. Alloys Compd.,* 2022, **895**, 162632.

[24] T. Chang, Q. Wei, Z. Wang, Y. Gao, B. Lian, X. Zhu, S. Cao, J. Zhao, B. Zou and R. Zeng, Phase-Selective Solution Synthesis of Cd-Based Perovskite Derivatives and Their Structure/Emission Modulation. *J. Phys. Chem. Lett.,* 2022, **13**, 3682-3690.

[25] Y. Jing, Y. Liu, X. Jiang, M. S. Molokeev, Z. Lin and Z. Xia, Sb3+ Dopant and

Halogen Substitution Triggered Highly Efficient and Tunable Emission in Lead-Free Metal Halide Single Crystals. *Chem. Mater.,* 2020, **32**, 5327-5334.

[26] C. Yang, F. Guo, Y. Zhang, X. Zhong, J. Feng, N. Wang and J. Wang, Luminescence Change from Orange to Blue for Zero-Dimensional Cs2InCl5(H2O) Metal Halides in Water and a New Post-doping Method. *Chem. Asian J.,* 2021, **16**, 1619-1625.

[27] M. Wang, J. Lyu, X. Qin, S.-W. Yang, X. Liu and G. Q. Xu, Direct Electron Transfer Enables Highly Efficient Dual Emission Modes of Mn2+-Doped Cs2Na1–xAgxBiCl6 Double Perovskites. *J. Phys. Chem. Lett.,* 2022, **13**, 9429-9434.

[28] B. Zhou, Z. Liu, S. Fang, J. Nie, H. Zhong, H. Hu, H. Li and Y. Shi, Emission Mechanism of Self-Trapped Excitons in Sb3+-Doped All-Inorganic Metal-Halide Perovskites. *J. Phys. Chem. Lett.,* 2022, **13**, 9140-9147.

[29] F. Liu, Y. Zhang, C. Ding, S. Kobayashi, T. Izuishi, N. Nakazawa, T. Toyoda, T. Ohta, S. Hayase, T. Minemoto, K. Yoshino, S. Dai and Q. Shen, Highly Luminescent Phase-Stable CsPbI3 Perovskite Quantum Dots Achieving Near 100% Absolute Photoluminescence Quantum Yield. *ACS Nano,* 2017, **11**, 10373-10383.

[30] S. Akhil, S. Biswas, M. Palabathuni, R. Singh and N. Mishra, Amine-Free Synthetic Route: An Emerging Approach to Making High-Quality Perovskite Nanocrystals for Futuristic Applications. *J. Phys. Chem. Lett.,* 2022, **13**, 9480-9493.

[31] Y. Wu, C.-M. Shi, L.-J. Xu, M. Yang and Z.-N. Chen, Reversible Luminescent Vapochromism of a Zero-Dimensional Sb3+-Doped Organic–Inorganic Hybrid. *J. Phys. Chem. Lett.,* 2021, **12**, 3288-3294.

[32] D.-S. Jiang, H. Jung and K. Ploog, Temperature Dependence of Photoluminescence from GaAs Single and Multiple Quantum-Well Heterostructures Grown by Molecular-Beam Epitaxy. *J. Appl. Phys.,* 1988, **64**, 1371-1377.

[33] J. Yu, J. Kong, W. Hao, X. Guo, H. He, W. R. Leow, Z. Liu, P. Cai, G. Qian, S. Li, X. Chen and X. Chen, Broadband Extrinsic Self-Trapped Exciton Emission in Sn-Doped 2D Lead-Halide Perovskites. *Adv. Mater.,* 2019, **31**, 1806385.

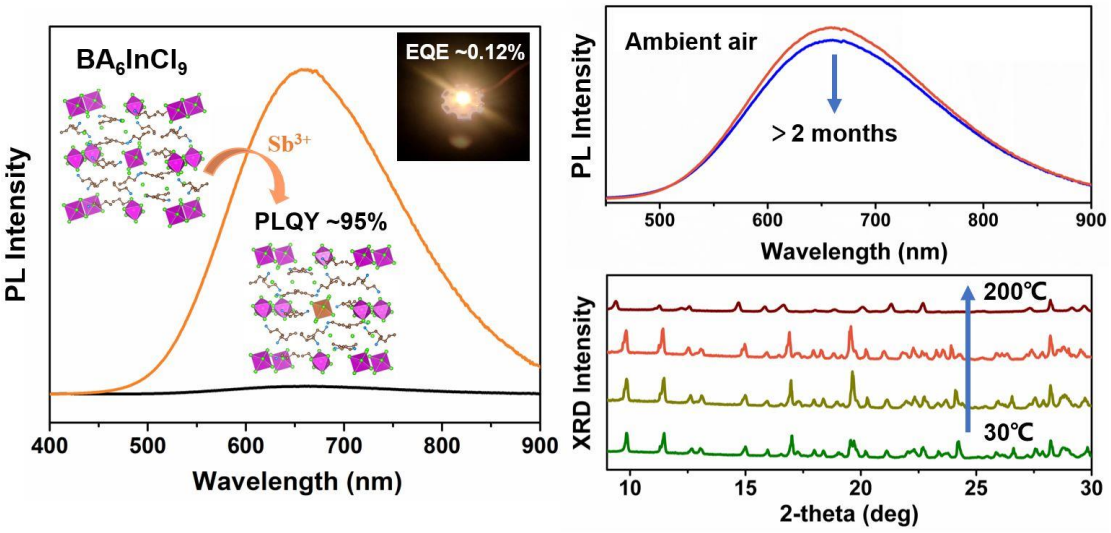
BA6InCl9
EQE ~0.12%
Sb3+
PLQY ~95%
PL Intensity
Wavelength (nm)
400
500
600
700
800
900
Ambient air
> 2 months
PL Intensity
Wavelength (nm)
500
600
700
800
900
200℃
30℃
XRD Intensity
2-theta (deg)
10
15
20
25
30

TOC